Particle Aggregation Dominates a Polymer-Induced Liquid-Precursor Process for Mineralization: Observations by Laser Light Scattering

Elaine DiMasi *, Tianbo Liu

Brookhaven National Laboratory, Upton NY 11973

Matthew J. Olszta, Laurie B. Gower **

University of Florida, Gainesville FL 32611

Abstract

A Polymer-Induced Liquid-Precursor (PILP) process for mineralization of calcium carbonate has been studied *in-situ* by laser light scattering. Static and dynamic light scattering data were obtained from $CaCl_2$ solutions containing poly(aspartic acid). Under these conditions calcium carbonate mineralizes through a liquid droplet precursor phase when the solution is exposed to the decomposition products of ammonium carbonate. Our measurements probe the integrated scatterer mass and the apparent hydrodynamic radius $R_{h,\mathrm{app}}$ of the droplets as they nucleate and coalesce. The data reveal three stages of the PILP process: an early stage of droplet growth to $R_{h,\mathrm{app}} \approx 250$ nm; a mid-time stage of fluctuations and polydispersity in particle size; and a final growth period where $R_{h,\mathrm{app}}$ increases from 350 nm to the micron scale. Aggregation of precursor droplets, rather than atom-by-atom growth, is the

dominant mechanism of mineral formation under these conditions.

Key words: biomineralization, amorphous calcium carbonate, laser light scattering

PACS: 81.10.-h, 81.10.-Dn

---

1 Introduction

The presence of biopolymers strongly affects mineralization from solution, through processes which are poorly understood but which are important in biomineralization and biomimetic materials science [1]. A number of different mechanisms have been described by which these macromolecules may affect the polytype or morphology of nucleating crystals, including stereochemical recognition [2,3], charge redistribution at the organic interface [4], promotion of crystal nucleation [5], inhibition of a particular polytype [6], and aggregation of proteins and crystallites [7]. The works cited above concern themselves with calcium carbonates, which are abundant as biogenic minerals and important to geochemistry. Much effort has been applied towards discerning relationships between the structural features of crystalline calcium carbonates and those of the organic matrix that control biomineralization.

A complete understanding of calcium carbonate biomineralization, however, must include the amorphous, hydrated $CaCO_3$ phase. Evidence of amorphous phases and transitory precursors in biominerals have been gaining more attention recently [8,9]. The amorphous phase is unstable relative to anhydrous $CaCO_3$ [10], converting to calcite under ambient laboratory conditions, and

* Email address for correspondence: dimasi@bnl.gov

**Email address for correspondence: lgowe@mse.ufl.edu

under the combination of vacuum and irradiation in electron microscopes. Thus this phase may go unobserved in experiments, making it difficult to test theories depending on structural or stereochemical aspects of *crystalline* mineral phases which in fact may not be present at the time of nucleation. Batch crystallization of $CaCO_3$ in the presence of polymer additives has recently been observed *in-situ* by Raman Spectroscopy [6], but the authors concentrated on distinguishing between crystalline $CaCO_3$ polymorphs and did not address the possibility of amorphous precursors. By contrast, *in-situ* observations by x-ray reflectivity [11] and small-angle x-ray scattering [12,13], have quantified the presence of nanoscale amorphous $CaCO_3$ films and particles during mineralization. Furthermore, acidic polypeptides such as poly(acrylic acid) and poly(aspartic acid) can also drive calcium carbonate mineralization through a liquid-liquid phase separation [14]. This Polymer-Induced Liquid-Precursor (PILP) process creates $CaCO_3$-rich droplets which can flow into confined spaces [15] and take the shape of surrounding boundary surfaces [16]. Upon dehydration, calcite crystals form which retain the fluidic shapes, yielding non-equilibrium morphologies which are evocative of biogenic calcium carbonate minerals. *Ex-situ* techniques such as electron microscopy have only been able to characterize the solid mineral product and not the fluidic precursor phase. Up to now, observations of the liquid-liquid phase separation have been achieved only through optical microscopy, where PILP particles were observed to reach dimensions of 2–4 microns in diameter. Given the smoothness of the mineral films the PILP process can create, we suspected that much smaller droplets might be present initially. Optical microscopy places a severe limitation on the resolution at which such nanoscopic phase separation may be characterized.

Here we report *in-situ* laser light scattering studies of the PILP process. Static light scattering measurements probe the integrated scatterer mass as a solution containing Ca and poly(aspartate) is exposed to the decomposition products of ammonium carbonate salts, and precipitates hydrated $CaCO_3$ droplets. In the dynamic light scattering analysis, the fluctuations in the scattered light are converted to diffusion times related to an apparent hydrodynamic radius $R_{h,\mathrm{app}}$ that characterizes the scattering particles. Our data reveal three stages of the PILP process: an early stage of droplet growth to $R_{h,\mathrm{app}} \approx 250$ nm; a mid-time stage of fluctuations and polydispersity in particle size; and a final growth period where $R_{h,\mathrm{app}}$ increases from 350 nm to the micron scale.

2 Materials and Methods

Samples consisted of 10 ml volumes in light scattering cuvettes, containing 20 mM $CaCl_2$ plus 20 μg/ml Poly-(α, β)-D,L-Aspartic Acid, $M_w = 8600$ g/mol (from Sigma). Into the cap of the light scattering vial were placed crushed ammonium carbonate crystals, separated from the sample volume by a Handiwrap film. The solutions precipitated $CaCO_3$ within the closed volumes as the decomposition products of $(NH_4)_2CO_3$ (carbon dioxide and ammonia gases) diffused through the film. Light scattering measurements were made with a Brookhaven Instruments spectrometer operating at a wavelength of 532 nm. Static intensity was recorded at a 90° scattering angle with occasional spot checks at 60°. Dynamic light scattering data was obtained by CONTIN analysis of photon correlation measurements made at these angles.

3 Results

The static scattered light intensity can be attributed to small, interacting particles in the Rayleigh–Gans–Debye analysis:

$$Hc/R_0 = 1/M_w(1 + A_2c) \,,$$

where R_0 is determined from the experimental scattered intensity; H is a function of the optical properties including the dependence of the index of refraction upon solute mass concentration c; M_w is a weight average molecular weight characterizing the scattering particles; and the second virial coefficient A_2 contains information about particle interactions. At low concentrations the measured intensity is approximately proportional to the total scatterer masses in solution. As Figure 1(a) shows, the raw intensity increases monotonically as droplets nucleate from solution. Because we did not control the gas diffusion rate in our experiments, the time dependences of our scattering data varied widely between different sample runs. Our interpretation of the scatterers as "droplets" rather than crystalline nuclei is supported by optical microscopy observations of additional reactions run under the same chemical conditions. Figure 2 is representative of the images taken, and shows the masses of droplets observable at the 10 μm scale after several hours, while only a few nascent calcite nuclei (which show color contrast under crossed polarizers) are present.

In the static light scattering experiment, a number of factors affect the measured intensity: the scatterer concentration and mass must both be expected to increase as particles precipitate and grow. In addition, as the carbonate species diffuse into the solution the optical constant H is affected. Unfortunately the variability of the data preclude our making any reasonable estimates

of the time-dependent carbonate concentration. It is impossible to say from static light scattering data alone whether particles are increasing only in concentration or also in mass, and whether they grow in a steady increase of size or by aggregating together.

Further information is obtained from dynamic light scattering, which was also acquired as a function of time throughout the reaction. In this measurement, the intensity–intensity time correlation function $G(\Gamma)$ is obtained by means of a digital correlator, yielding the distribution of apparent diffusion coefficients. The diffusion coefficient can then be related to an apparent hydrodynamic radius $R_{h,\mathrm{app}}$ by the Stokes-Einstein theory [17]. Representative particle size distributions are shown in Figure 1(b). The $R_{h,\mathrm{app}}$ distributions have different character in different time intervals. At early times, hydrodynamic radii are in the range 100–200 nm. Distributions are typically sharp, with intensity appearing in only one or two channels of the correlator. Midway into each experiment, the distribution of $R_{h,\mathrm{app}}$ changes, with peaks becoming broadened, noisy, and occasionally having a bimodal distribution. Values of $R_{h,\mathrm{app}}$ measured during this mid-time regime have values between 100 and 450 nm. At late times, the hydrodynamic radius is observed to increase from about 300 to 800 nm, at which point the particles have reached the micron scale and are not well characterized by light scattering.

The $R_{h,\mathrm{app}}$ values we obtained for each data point in three different runs are compiled in Figure 3, where $R_{h,\mathrm{app}}$ is plotted against time. In experiment (a), a roughly monotonic increase in $R_{h,\mathrm{app}}$ from 120 to 240 nm is observed for $t < 35$ minutes. After this, a bimodal $R_{h,\mathrm{app}}$ distribution appears (note the two $R_{h,\mathrm{app}}$ points for $t = 30$ min) and the $R_{h,\mathrm{app}}$ distributions are broad and noisy, fluctuating between 150 and 450 nm. Experiments (b) and (c) do not exhibit

an early period of growth, but start with a fluctuating $R_{h,\mathrm{app}}$ distribution in a similar range of $R_{h,\mathrm{app}} \leq 450$ nm. At late times in experiments (b) and (c) the particle size begins to increase, again monotonically, from 300 to 800 nm.

4 Discussion

Our observations of this Polymer-Induced Liquid-Precursor (PILP) process reveal three distinct stages in the nucleation and growth of amorphous mineral-precursor particles. Diffusion of ammonia and carbon dioxide gases into the solution precipitates $CaCO_3$ in droplet form due to the presence of the polymer. As mentioned above, this unknown and uncontrolled diffusion rate prevents a quantitative comparison between time points or reaction rates of individual experiments. Because the time-dependent solute concentration is not known, the static scattering intensities cannot be converted into individual particle masses.

The large size of the particles also presents difficulties in quantitative interpretation, for two reasons. The first is that the ratio of the measured 90° scattered intensity to that at 0°, from which the scatterer mass would be derived, becomes very large and is too sensitive to the choice of particle radius and dispersity used for the analysis. The second is that the extrapolation of the apparent hydrodynamic radius $R_{h,\mathrm{app}}$ to a true particle radius becomes unreliable. Our efforts toward such analysis have convinced us that the uncertainties in some of these quantities span nearly an order of magnitude. For these reasons we have not tried to obtain more quantitative information about particle densities, and so we cannot determine for example the extent to which the particles are hydrated at any given stage of growth.

However, qualitative assessments of the particles are illuminating. First we consider the early growth stage of experiment (a). From $t = 17$ to $t = 32$ minutes, $R_{h,\mathrm{app}}$ increases from 112 to 258 nm, about a factor of two, while the normalized static scattered intensity also increases by about a factor of two. This suggests that the size increase is due principally to particle aggregation rather than continued precipitation from solution. If the particles were doubling in size due to more ions coming out of solution, each particle would increase its mass eightfold and this would have to be reflected in an eightfold increase in the total scatterer mass. Instead, the total mass has only doubled. Therefore, we surmise that particle aggregation is the predominant process during the times when particles are 100-250 nm in size.

In mid-time regions, the distribution of particle sizes is roughly the same at the beginning and end of the interval. This generalization can be made for all three experimental runs shown in Figure 3 as well as for additional experiments we performed under varied conditions (data not shown). Although the particle size distribution was always the same for the duration of any mid-time interval we studied, the time dependence of the accompanying static data varied considerably. For example, in the experiment of Figure 3(a) the static intensity increases by a factor of 5 while that in Figure 3(c) the measurements span a factor of 100, over comparable 50-minute time intervals. This interval therefore may reflect the continual addition of reactants to the solution, which occurs at variable rates. As long as the solution is supersaturated, the gas diffusion process provides a continuous source of the smallest particles, which aggregate as they encounter each other.

At this point in the discussion, we want to keep in mind that along with aggregation, the particles eventually undergo a stage of dehydration. Our ob-

servations of micron-sized droplets by optical microscopy have shown that the droplets ultimately crystallize as calcite, having evicted the waters of hydration while maintaining their overall fluidic shapes [14]. As judged by comparison between *in-situ* optical microscopy and SEM studies of PILP droplets in our previous work, no overall volume change can be discerned, and so we expect that these droplets must release most of the water at earlier times. Dehydration alone, of a static concentration of scatterers, would be expected to decrease the total scatterer mass, an effect we cannot observe independently in the presence of the other time-dependent events in these experiments. Dehydration and densification could certainly contribute to the fluctuations observed. The bimodal size distributions and persistence of smaller particles following the appearance of larger ones, could also results from hydrated $CaCO_3$ droplets which have evicted enough water to shrink in size.

In the late stage of experiment (c), $t = 120$–180 minutes, $R_{h,\mathrm{app}}$ increases from 300 to 800 nm (factor of 2.6), while the static intensity increases by a factor 1.5. Though we note that at such large sizes the difference between $R_{h,\mathrm{app}}$ and the true particle size becomes significant, and one should be cautious in comparing $R_{h,\mathrm{app}}$ values, here again the principal reason for the size increase must be aggregation. In our experiments we never observe increases of total scatterer mass that scale with $(R_{h,\mathrm{app}})^3$. Our optical microscopy experiments, conducted over a range of similar conditions, are compatible with this conclusion as many instances of micron-scale particle aggregation have been observed, as suggested by the massed droplets in Figure 2. It is interesting to note that others have observed trails of aggregated droplet shapes in AFM studies of calcite growth in the presence of acidic proteins extracted from the calcitic shells of coccolithophores [18] and from red abalone shell [19]. The droplets,

presumed to be crystal nuclei, follow ribbons of protein in the former reference and step edges in the latter. In both cases, the propensity of the protein to bind calcium, leading to local concentration fluctuations, is acknowledged to play an important role. In AFM studies, the morphology and kinetics of crystallization at step edges are most readily observed, and interpreted in terms of classical nucleation and growth mechanisms. However, our solution-phase experiments prove that the acidic polymers induce phase separation in the absence of pre-existing calcite surfaces. This leads us to suggest that the acidic polymer, and the accompanying sequestration of cations and counter-anions near it, may allow the system to phase separate through a spinodal decomposition mechanism, either at a crystal surface or in solution. In the latter case the mineral-rich droplets may then diffuse to the available surfaces, leading in the case of a straight step edge to a convoluted morphology for that edge. A combined experimental and theoretical effort to test this model might be very illuminating — neither the present light scattering nor the reported AFM studies are really adequate to fully characterize these 3-phase systems of minerals and proteins in solution.

In this context, it is interesting to compare recent observations by small-angle x-ray scattering (SAXS) of $CaCO_3$ nucleation from solution in the *absence* of polymer.[12] Here, rapid mixing of $CaCl_2$ and Na_2CO_3 produced a high super-saturation and the resulting colloidal $CaCO_3$ particles were observed by time-resolved synchrotron measurements, one objective being to identify transient metastable $CaCO_3$ species. The SAXS study observes particles which achieve sizes of 133 nm in 100 seconds. In subsequent studies, combined small- and wide-angle scattering demonstrated that the amorphous particles re-dissolve prior to the formation of calcite particles [13]. By contrast the presence of

polymer in our study substantially inhibits particle growth, although it also enables larger clusters to form. Particle densities estimated by SAXS were found to be about half that expected for anhydrous $CaCO_3$ species and this was attributed to a hydrated, amorphous precursor phase [12,13]. An almost identical observation has been made by our group for polymer-induced $CaCO_3$ precursor films nucleated at fatty acid monolayers at the water surface and studied by *in-situ* synchrotron x-ray reflectivity [11]. In the case of the surface films, increased proportions of polymer can lengthen the life of the precursor film, but do not strongly affect the kinetics of its growth or the subsequent transformation to calcite [DiMasi *et al*, manuscripts in preparation].

Combining the available observations from experiments with and without polymer additives, it appears that the hydrated precursor might be ubiquitous as a stage in $CaCO_3$ mineralization, but that an acidic polypeptide may be necessary to stabilize this precursor phase long enough for its fluidic morphology to be incorporated into the shape of the final crystalline product. It is this role that we believe is the most relevant to biomineralization processes, where proteins direct the minerals to form the specific complex morphologies that are incorporated into the well-known hierarchical structures. Illuminating the mechanisms by which organic species direct mineralization is the objective of our future studies on polymer-induced mineral precursor phases.

5 Acknowledgments

We acknowledge support from the Particle Engineering Research Center (PERC) at the University of Florida,the Industrial Partners of PERC, and the National Science Foundation (Grants EEC-94-02989 and DMR-0094209). Brookhaven

National Laboratory is supported under U.S. DOE Contract DE-AC02-98CH10886.

References

[1] N. Dan, Synthesis of hierarchical materials, TIBTECH 18.

[2] P. J. J. A. Buijnsters, J. J. J. M. Donners, S. J. Hill, B. R. Heywood, R. J. M. Nolte, B. Zwanenburg, N. A. J. M. Sommerdijk, Langmuir 17 (2001) 3623.

[3] Y.-J. Han, J. Aizenberg, Face-selective nucleation of calcite on self-assembled monolayers of alkanethiols: effect of the parity of the alkyl chain, Angew. Chemie 42 (2003) 3668.

[4] M. J. Lochhead, S. R. Letellier, V. Vogel, Assessing the role of interfacial electrostatics in oriented mineral nucleation at charged organic monolayers, J. Phys. Chem. B 101 (1997) 10821.

[5] L. Pach, Z. Hrabe, S. Komarneni, R. Roy, Controlled crystallization of vaterite from viscous solutions of organic colloids, J. Mater Res. 5.

[6] P. Agarwal, K. A. Bergland, in situ monitoring of calcium carbonate polymorphs during batch crystallization in the presence of polymeric additives using raman spectroscopy, Langmuir 18 (2003) 8364.

[7] R. Lakshminarayanan, R. M. Kini, S. Valiyaveettil, Investigation of the role of ansocalcin in the biomineralization in goose eggshell matrix, PNAS 99.

[8] E. Beniash, J. Aizenberg, L. Addadi, S. Weiner, Amorphous calcium carbonate transforms into calcite during sea urchin larval spicule growth, Proc. R. Soc. Lond. B (1997) 461.

[9] W. F., Matrix and mineral in the sea urchin larval skeleton, J. Struct. Biol. 126 (1999) 216.

[10] R. Brooks, L. M. CLark, E. F. Thurston, calcium carbonate and its hydrates, Proc. Royal Soc. London 243A (1950) 145.

[11] E. DiMasi, V. M. Patel, M. Sivakumar, M. J. Olszta, Y. P. Yang, L. B. Gower, Polymer-controlled growth rate of an amorphous mineral film nucleated at a fatty acid monolayer, Langmuir 18 (2002) 8902.

[12] J. Bolze, B. Peng, N. Dingenouts, P. Panine, T. Narayanan, M. Ballauff, Formation and growth of amorphous colloidal caco3 precursor particles as detected by time-resolved saxs, Langmuir 18 (2002) 8364.

[13] D. Pontoni, J. Bolze, N. Dingenouts, T. Narayanan, M. Ballauff, Crystallization of calcium carbonate observed in-situ by combined small- and wide-angle x-ray scattering, J. Phys. Chem. B 107 (2003) 5123.

[14] L. B. Gower, D. J. Odom, Deposition of calcium carbonate films by a polymer-induced liquid-precursor (pilp) process., J. Crystal Growth 210 (2000) 719.

[15] M. J. Olszta, E. P. Douglas, L. B. Gower, Intrafibrillar mineralization of collagen using a liquid-phase mineral precursor, in: Materials Inspired by Biology, Vol. 774, The Materials Research Society, Warrendale PA, 2003, p. 127.

[16] Y. Kim, L. B. Gower, Formation of complex non-equilibrium morphologies of calcite via biomimetic processing, in: Materials Inspired by Biology, Vol. 774, The Materials Research Society, Warrendale PA, 2003, p. 141.

[17] T. Liu, R. Rulkens, G. Wegner, B. Chu, laser light scattering study of a rigid-rod polyelectrolyte, Macromolecules 31 (1998) 6119.

[18] B. L. Smith, G. T. Paloczi, P. K. Hansma, R. P. Levine, Discerning nature's mechanism for making complex biocomposite crystals, J. Cryst. Growth 211.

[19] D. Walters, B. L. Smith, A. M. Belcher, G. T. Paloczi, G. D. Stucky, D. E. Morse, P. K. Hansma, Modification of calcite growth by abalone shell proteins: An atomic force microscope study, Biophysical Journal 72 (1997) 1425.

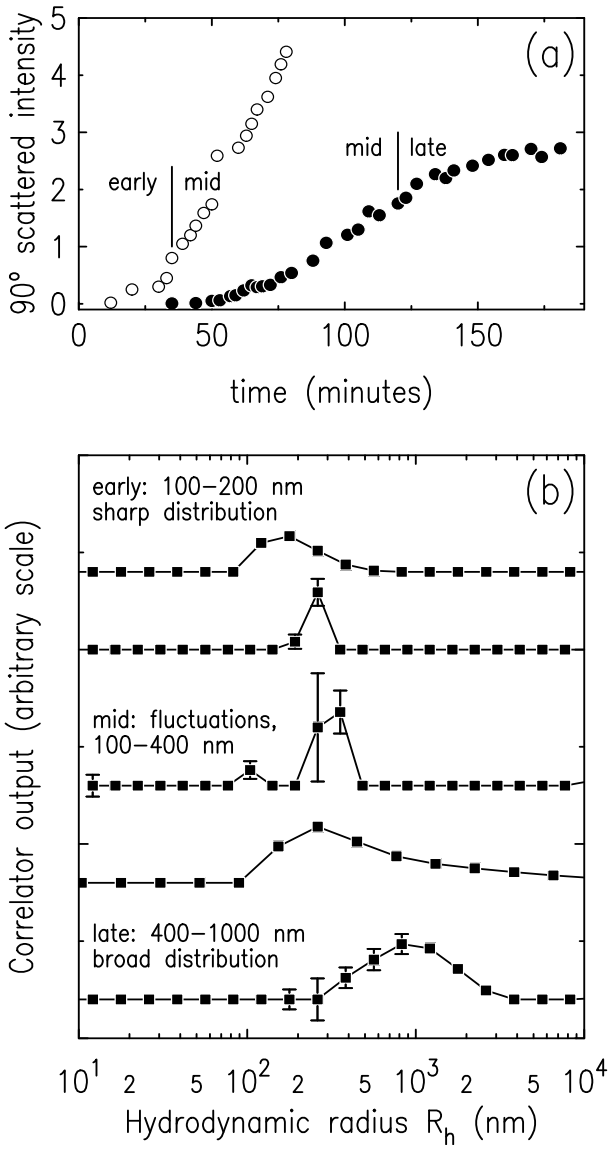

Fig. 1. (a) Raw intensities for static light scattering data, at 90° scattering angle. Lines at the inflection points, separating early, mid and late times, are defined from the DLS data in Figure 2 (see text). Open and closed circles correspond to runs (a) and (c) of Figure 2. (b) Selected correlator output scans from runs (a) (early, mid) and (c) (late). At early times, the smallest hydrodynamic radii $R_{h,\mathrm{app}} = 100$–300 nm are observed, often with sharp distributions. Intermediate times show broadened distributions and occasional bimodal distributions in particle size. At late times broad distributions of large particles are observed.

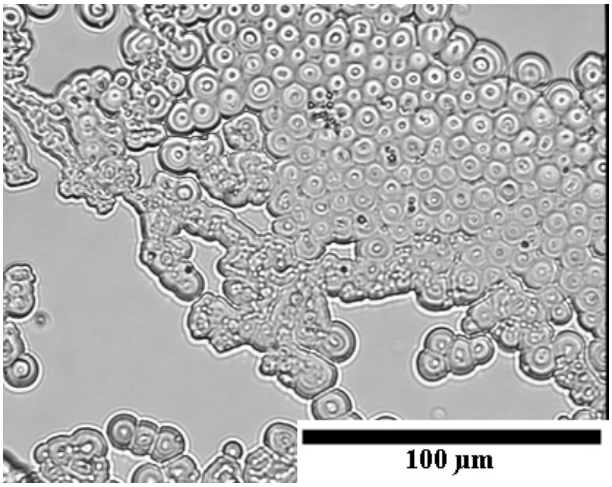

Fig. 2. Optical micrograph (20x) of PILP droplets formed under conditions similar to those used for light scattering experiments. Droplets aggregate, but only partially coalesce, when reaching such a large size, presumably due to the partial dehydration and solidifcation that occurs by this late stage. Image acquired 4.5 hours after beginning exposure of the $CaCl_2$/Pasp solution to $(NH_4)_2CO_3$ salt vapors.

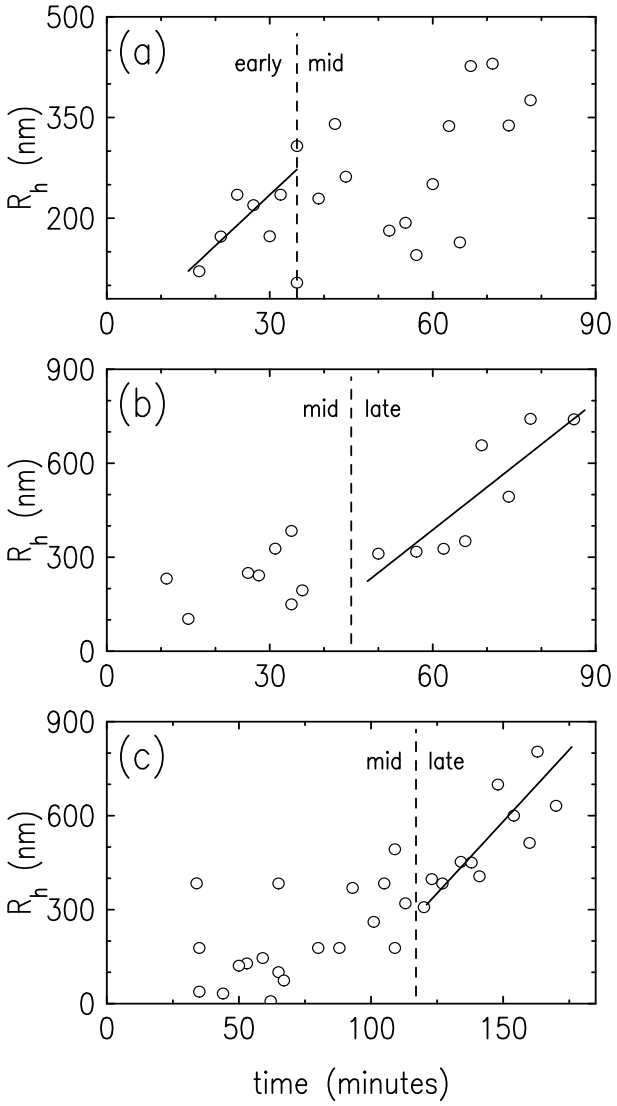

Fig. 3. Apparent hydrodynamic radius $R_{h,\mathrm{app}}$ inferred from dynamic light scattering measurements vs. time for each of three separate experimental runs. (a) Run characterized by an early stage of particle growth followed by a mid-time regime of large fluctuations and bimodal distributions in $R_{h,\mathrm{app}}$. Bimodal distributions in $R_{h,\mathrm{app}}$ are indicated by two separate data points at different $R_{h,\mathrm{app}}$ plotted at the same time point. (b),(c) Runs characterized by observations of fluctuating $R_{h,\mathrm{app}}$ followed by growth from 300 to 800 nm. Lines in all panels are guides for the eye.